CCFE-PR(17)69

S. L. Dudarev and Pui-Wai Ma

Elastic fields, dipole tensors, and interaction between self-interstitial atom defects in bcc transition metals

Elastic fields, dipole tensors, and interaction between self-interstitial atom defects in bcc transition metals

S. L. Dudarev and Pui-Wai Ma

Culham Centre for Fusion Energy, UK Atomic Energy Authority, Abingdon, Oxfordshire OX14 3DB, United Kingdom

Elastic fields, dipole tensors, and interaction between self-interstitial atom defects in bcc transition metals.

S. L. Dudarev and Pui-Wai Ma
*Culham Centre for Fusion Energy, UK Atomic Energy Authority, Abingdon, Oxfordshire OX14 3DB, United Kingdom**

Density functional theory (DFT) calculations show that self-interstitial atom defects in non-magnetic body-centred cubic (bcc) metals adopt strongly anisotropic configurations, elongated in the ⟨111⟩ direction[1–4]. Elastic distortions, associated with such anisotropic defect configurations, appear similar to the distortions around small prismatic dislocation loops, although the extent of this similarity has not been quantified. We derive analytical formulae for the dipole tensors of ⟨111⟩ defects in the isotropic and anisotropic elasticity approximations. These expressions show that, in addition to the prismatic dislocation loop-like character, the elastic field of a ⟨111⟩ defect also has a significant isotropic dilatation component. Using a multi-scale approach, which combines DFT calculations with elasticity, we parameterize dipole tensors of defects for all the non-magnetic bcc transition metals. This enables quantitative evaluation of the energy of elastic interaction between the defects, which also shows that in a periodic three-dimensional arrangement, long-range elastic interaction between a defect and all its images favours a ⟨111⟩ orientation of the defect.

I. INTRODUCTION

Strongly anisotropic self-interstitial defect configurations form spontaneously in body-centred cubic metals like sodium[5] or tungsten[2–4] if an extra atom, identical to the atoms of the host material, is inserted in the crystal lattice and the resulting structure is relaxed into the lowest energy configuration. Such anisotropic 'crowdion' or 'dumbbell' defects are produced simultaneously with vacancies in high-energy collision cascade events[6,7] as Frenkel pairs. The defects have a characteristic anisotropic lattice strain associated with them, illustrated in Fig. 1. The figure shows a self-interstitial defect in tungsten, where the positions of atoms were determined by a DFT calculation.

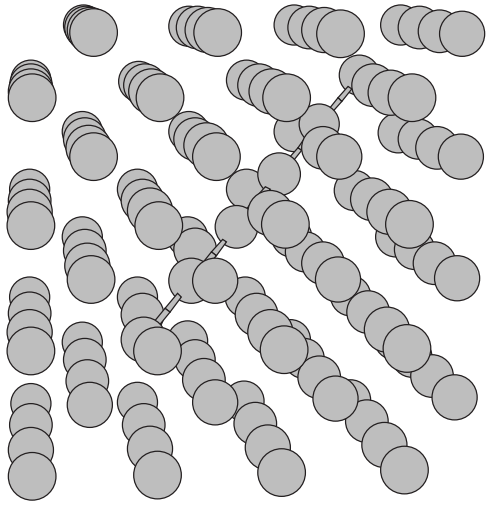

FIG. 1: Atomic structure of a self-interstitial atom defect in tungsten, where the orientation of the axis of the defect is close to the [111] direction. Atomic bonds are shown for the atoms that are significantly closer to each other than atoms in a perfect lattice.

Properties of self-interstitial atom (SIA) defects are significantly different from those of vacancies. For example, diffusion of vacancies is thermally activated and observed only at relatively high temperatures, above 650K in tungsten[8], whereas in the same material the SIA crowdion defects are mobile at temperatures that are as low as several Kelvin[9,10].

The equilibrium structure[2–4] and modes of Brownian motion (diffusion)[10–13] of individual SIA defects in body-centred transition metals are now well established. Yet, there is still no regular approach to the treatment of evolution of ensembles of such defects, including the effect of elastic interaction between the defects. The difficulty appears fundamental, illustrating the lack of a sufficiently general formalism linking discrete atomistic representation of structure nano-scale defects with continuum elasticity.

Recently, we have derived tractable analytical expressions[14] for the energy of elastic interaction between two dislocation loops, and between a dislocation loop and a dilatation centre, for example a vacancy cluster. These equations use the notion of elastic dipole tensor of a dislocation loop, expressed in terms of its Burgers vector, its area, and the unit normal vector to the habit plane of the loop. However, the analysis is based entirely on the treatment of dislocations in elastic continuum, and cannot be applied to point defects.

Here we aim to explore defects that are too small to be treated using the notions of macroscopic elasticity[15]. Whereas it is in principle possible to describe elastic fields of nano-scale defects using dipole tensors computed numerically[18], in practice this is not convenient, as numerical calculations have to be repeated every time when a defect changes its configuration. For example, this occurs frequently when a self-interstitial defect migrates, as it alters the direction of its motion[3,16]. The effect of applied strain on SIA defects in α-Fe was explored using DFT recently in Ref.[17]. In this work, we show how to parameterize the dipole tensor of a defect using certain

invariant quantities, for example its elastic relaxation volume, as opposed to dynamic variables that may evolve as functions of time. Dynamic parameters here are the coordinates of the defect[12,13] or the unit vector characterizing the anisotropy of its structure.

We start by deriving an analytical expression for the dipole tensor of a dislocation loop, and then considering the limit of an infinitesimally small loop size. Surprisingly, we find that this seemingly natural approach results in a prediction for the dipole tensor of a point defect that does not agree with numerical calculations even for defects in tungsten, which is well described by isotropic elasticity theory. We then derive an analytical representation for the dipole tensor of a defect using a two-parameter tensorial form, which shows that in addition to a pure prismatic dislocation loop character, the elastic field of a crowdion also contains a significant *isotropic* dilatation component. We also derive an analytical expression for the energy of interaction between two crowdion defects, and between a crowdion defect and a dilatation centre, for example a vacancy cluster. To illustrate applications of the new formalism, we evaluate the energy of interaction between crowdions ordered in the form of a periodic super-lattice often encountered in DFT calculations. Surprisingly, we discover that the energy minimum of such periodic configuration corresponds to an orientation of the directional unit vector of the crowdions that is close to a $\langle 111 \rangle$ direction. This unusual symmetry-breaking effect, noted earlier in the context of density functional theory calculations, see e.g. Ref. 19, results from elastic interaction between a crowdion and all its images in a simulation involving periodic boundary conditions.

The analysis given below highlights the part that the notion of elastic fields of point defects plays in the multiscale treatment of microstructural evolution of materials exposed to a flux of high-energy particles. On the one hand, point defects are the elementary building blocks of dislocations and vacancy clusters forming under irradiation. On the other hand, the structure and properties of elementary point defects are strongly influenced by the discreteness of the lattice, making an elasticity-based treatment, highlighting similarities and differences between defects and dislocations, critical to the development of lattice-continuum multi-scale models.

II. ELASTIC DIPOLE TENSOR OF A DISLOCATION LOOP AND A CROWDION POINT DEFECT

The energy of interaction between a defect and external homogeneous strain field ϵ_{ij}^{ext}, according to equation (4.99) of Ref. 18, is

$$E = -P_{ij}\epsilon_{ij}^{ext}. \tag{1}$$

Here P_{ij} is the elastic dipole tensor of the defect, and ϵ_{ji}^{ext} is a slowly varying function of spatial coordinates. Another application of the notion of elastic dipole tensors is in a calculation of the energy of elastic interaction between any two defects a and b, given by

$$E_{int}^{ab} = P_{ij}^{a} P_{kl}^{b} \frac{\partial}{\partial x_j} \frac{\partial}{\partial x_l} G_{ik}(\mathbf{r}), \tag{2}$$

where P_{ij}^{a} and P_{ij}^{b} are the dipole tensors of the two defects, $\mathbf{r} = \mathbf{r}_a - \mathbf{r}_b$, and x_i are the Cartesian components of $\mathbf{r}$. Green's function of elasticity equations $G_{ik}(\mathbf{r})$ in the isotropic elasticity approximation has the form[20]

$$G_{ik}(\mathbf{r}) = \frac{1}{16\pi\mu(1-\nu)r}\left[(3-4\nu)\delta_{ik} + \frac{x_i x_k}{r^2}\right], \tag{3}$$

where μ is the shear modulus and ν is the Poisson ratio.

In the limit where the external strain field is homogeneous and independent of spatial coordinates, equation (1) can be applied not only to a small defect but also to a dislocation loop of arbitrary size. In this limit, the dipole tensor of a dislocation loop can be found by comparing (1) with equation (4-41) of Ref. 15, namely

$$E = -\int b_i \sigma_{ij}^{ext} dA_j, \tag{4}$$

where $\mathbf{b}$ is the Burgers vector of the loop, σ_{ij}^{ext} is the stress tensor of external elastic field, and integration over dA_j is performed over an arbitrary surface bounding the loop. Using Hooke's law

$$\sigma_{ij} = C_{ijkl}\epsilon_{kl}, \tag{5}$$

and combining equations (4) and (1), we arrive at[14]

$$P_{ij} = C_{ijkl} b_k A_l, \tag{6}$$

where A_l is a Cartesian component of the vector area $\mathbf{A}$ of the loop, which may be conveniently expressed as a contour integral over the perimeter of the loop as[21]

$$\mathbf{A} = \frac{1}{2}\oint (\mathbf{r} \times d\mathbf{l}). \tag{7}$$

In the isotropic elasticity approximation, where

$$C_{ijkl} = \mu\frac{2\nu}{1-2\nu}\delta_{ij}\delta_{kl} + \mu\left(\delta_{ik}\delta_{jl} + \delta_{il}\delta_{kj}\right), \tag{8}$$

the elastic dipole tensor of a dislocation loop acquires the form[14]

$$P_{ij} = \mu\left[(b_i A_j + A_i b_j) + \frac{2\nu}{1-2\nu}(\boldsymbol{b}\cdot\boldsymbol{A})\delta_{ij}\right]. \tag{9}$$

The elastic relaxation volume Ω_{rel}, which is a quantity characterizing the degree of macroscopic expansion or contraction (swelling) of the material due to the presence of a defect in it, in the isotropic elasticity approximation under *traction-free boundary conditions* equals

$$\Omega_{rel} = \frac{(1-2\nu)}{2\mu(1+\nu)}\mathrm{Tr}P_{ij}. \tag{10}$$

Substituting (9) into (10), we find the relaxation volume of a dislocation loop[14]

$$\Omega_{rel} = (\mathbf{b}\cdot\mathbf{A}) = \frac{1}{2}\oint \mathbf{b}\cdot(\mathbf{r}\times d\mathbf{l}). \tag{11}$$

This equation remains valid even if the material is elastically anisotropic. In anisotropic elasticity, the elastic relaxation volume of a defect is given by the trace of a tensor product[18]

$$\Omega_{rel} = S_{kkij}P_{ij}, \tag{12}$$

where $\hat{S}=\hat{C}^{-1}$ is the tensor of elastic compliance[22]. Formula (11) for the relaxation volume of a dislocation loop then follows from the substitution of (6) into (12).

The relaxation volume of a dislocation loop (11) does not depend on elastic properties or the position of the loop in the material. It is a purely geometric property of the dislocation line forming the loop. In particular, the relaxation volume does not depend on the distance between the dislocation loop and the surface, and equation (11) remains valid irrespectively of the shape of the crystal, provided that the traction-free boundary conditions are satisfied.

It is also useful to derive an expression for the rate of variation of the relaxation volume of a dislocation loop as a function of time. The derivative of the relaxation volume of the loop is

$$\frac{d\Omega_{rel}}{dt} = \oint \mathbf{v}\cdot(d\mathbf{l}\times\mathbf{b}), \tag{13}$$

where $\mathbf{v}$ is the velocity of segment $d\mathbf{l}$ at the loop perimeter. If a dislocation loop evolves through self-climb[23], the relaxation volume of a dislocation loop remains constant and $d\Omega_{rel}/dt = 0$. On the other hand, under the conditions of vacancy-mediated climb, the rate of variation of relaxation volume can be positive or negative, depending on the vacancy or self-interstitial nature of the loop[24].

The elastic field of an isotropic point defect, for example a vacancy, is characterized by only one parameter, the elastic relaxation volume. The elastic dipole tensor of an isotropic point defect can be written as

$$P_{ij} = \frac{\Omega_{rel}}{3}C_{ijkl}\delta_{kl}. \tag{14}$$

In a cubic crystal this can be simplified further. Using the Voigt notations[22], from (14) we find

$$P_{ij} = \frac{\Omega_{rel}}{3}(C_{11}+2C_{12})\delta_{ij}, \tag{15}$$

which in the isotropic elasticity limit, where $C_{11} = 2\mu(1-\nu)/(1-2\nu)$ and $C_{12} = 2\mu\nu/(1-2\nu)$, becomes[14]

$$P_{ij} = \frac{2\mu\Omega_{rel}}{3}\frac{1+\nu}{1-2\nu}\delta_{ij}. \tag{16}$$

To describe a linear anisotropic defect structure, like a crowdion shown in Fig. 1, we define a vector $\mathbf{n}$ characterizing the orientation of the axis of the defect, and write

$$P_{ij} = C_{ijkl}\left(\Omega^{(1)}n_k n_l + \frac{\Omega^{(2)}}{3}\delta_{kl}\right). \tag{17}$$

The above expression is a generalization of (6) and (14) to the case where the structure of the defect is characterized by a unit vector $\mathbf{n}$, out of which we construct a symmetric two-index tensor $n_k n_l$, entering the expression for the dipole tensor analogously to how the Kroneker symbol δ_{kl} enters equation (14).

Substituting (17) into (12), we see that the total relaxation volume of a point defect is

$$\Omega_{rel} = \Omega^{(1)} + \Omega^{(2)}. \tag{18}$$

The two parameters $\Omega^{(1)}$ and $\Omega^{(2)}$ are measures of the relative weight of anisotropic and isotropic components of the elastic field of a defect. In the isotropic elasticity limit, where tensor C_{ijkl} is given by equation (8), formula (17) becomes

$$P_{ij} = 2\mu\Omega^{(1)}n_i n_j + 2\mu\left[\frac{\nu}{1-2\nu}\Omega^{(1)} + \frac{1}{3}\frac{1+\nu}{1-2\nu}\Omega^{(2)}\right]\delta_{ij}. \tag{19}$$

It is instructive to compare equation (19) for the elastic dipole tensor of a $\langle 111\rangle$ crowdion defect, and equation (9) for the elastic dipole tensor of a dislocation loop. In the pure prismatic loop limit, where the Burgers vector of the loop $\mathbf{b}$ is collinear with the loop area vector $\mathbf{A}$, equation (9) can be written as

$$P_{ij} = 2\mu bA\left[n_i n_j + \frac{\nu}{1-2\nu}\delta_{ij}\right]. \tag{20}$$

Here, unit vector $\mathbf{n}$ defines the direction of both $\mathbf{b}$ *and* $\mathbf{A}$. While the similarity between (20) and (19) is apparent, there is also a fundamental difference between the two cases. The dipole tensor of a pure prismatic dislocation loop (20) is fully defined by a single parameter, the product bA, which in this case is the relaxation volume of the loop. On the other hand, defining the elastic dipole tensor (17) of a crowdion defect requires two parameters, where parameter $\Omega^{(2)}$ describes the dilatation component of the elastic field of the defect, absent in the case of a pure prismatic dislocation loop. Numerical calculations of elastic dipole tensors of point defects in various bcc transition metals summarized in the next section show that the dilatation component of elastic fields of defects is non-negligible, suggesting that a crowdion point defect is an entity fundamentally dissimilar from an infinitesimally small dislocation loop.

III. DENSITY FUNCTIONAL THEORY CALCULATION OF ELASTIC DIPOLE TENSORS

The dipole tensor of a defect can be computed using density functional theory, or empirical interatomic po-

tentials, by evaluating the response of a simulation cell to external applied strain, namely[25,26],

$$P_{ij} = V_{cell}(C_{ijkl}\epsilon_{kl}^{app} - \langle\sigma_{ij}\rangle). \quad (21)$$

Here V_{cell} is the volume of the simulation cell, ϵ_{ij}^{app} is the external applied strain, and $\langle\sigma_{ij}\rangle$ is the total macroscopic stress of the simulation box. Note that the right-hand side of (21) vanishes in accordance with Hooke's law if the cell contains no defect.

To rationalize formula (21) we note that the elastic strain energy of a defect in an infinite medium is given by the volume integral

$$E_D = \frac{1}{2}\int_V \sigma_{ij}\epsilon_{ij}dV, \quad (22)$$

$$= \frac{1}{2}\int_V C_{ijkl}\epsilon_{kl}\epsilon_{ij}dV, \quad (23)$$

where integration is performed over the entire space. In the presence of infinitesimal external strain ϵ_{ij}^{ext}, E_D can be written in the linear approximation in ϵ_{ij}^{ext} as

$$E_D(\epsilon_{ij}^{ext}) = E_D(\epsilon_{ij}^{ext}=0) + \left(\frac{\delta E_D}{\delta\epsilon_{ij}^{ext}}\right)_{\epsilon_{ij}^{ext}=0}\epsilon_{ij}^{ext}. \quad (24)$$

Comparing this with equation (1), we find

$$P_{ij} = -\left(\frac{\delta E_D}{\delta\epsilon_{ij}^{ext}}\right)_{\epsilon_{ij}^{ext}=0} \quad (25)$$

$$= -\int_V C_{ijkl}\epsilon_{kl}^D dV = -\int_V \sigma_{ij}^D dV, \quad (26)$$

where ϵ_{ij}^D is the strain and σ_{ij}^D is the stress resulting from the presence of a defect in the simulation cell. The dipole tensor equals the negative of the volume integral of stress induced by the defect.

Numerical simulations often involve the use of periodic boundary conditions. In effect, the use of periodic boundary conditions amounts to simulating an infinite number of defects, each occupying a volume element equivalent to the volume of the simulation cell. The dipole tensor can be computed from the macro-stress associated with the simulation cell, namely

$$P_{ij} = -\int_{V_{cell}}\sigma_{ij}dV = -V_{cell}\langle\sigma_{ij}\rangle. \quad (27)$$

Equations (26) and (27) are equivalent in the linear elasticity approximation. This can be proven as follows. Assume that N identical defects are distributed in an infinite medium. In the limit $N\to\infty$, the total stress is the same as the total stress induced by a defect plus its periodic images

$$N\int_V \sigma_{ij}^D dV = \int_V \sigma_{ij}^D dV + \sum_n \int_V \sigma_{ij}^{I,n} dV, \quad (28)$$

where $\sigma_{ij}^{I,n}$ is the stress induced by its n^{th} periodic image. Dividing both sides of the above equation by N, we find

$$\int_V \sigma_{ij}^D dV = \frac{1}{N}\int_V \left(\sigma_{ij}^D + \sum_n \sigma_{ij}^{I,n}\right) dV, \quad (29)$$

$$= \int_{V_{cell}} \sigma_{ij}dV. \quad (30)$$

This is because the stress in a simulation cell is equivalent to stress within any periodically translated cell, and the stress within the cell is a linear sum of stresses induced by the defect and all its images.

In principle, the size of the simulation box containing a defect should remain the same as the size of the cell corresponding to the perfect lattice. If the size of the simulation cell containing a defect is different from the perfect lattice case, then the cell is strained, and to compute the dipole tensor one should also take into account the first term in (21).

IV. NUMERICAL RESULTS

To evaluate elastic dipole tensors, we performed *ab initio* calculations of the most stable defect configurations in vanadium, niobium, tantalum, molybdenum and tungsten. In all the non-magnetic bcc transition metals, the $\langle 111\rangle$ configuration has the lowest formation energy in comparison to other self-interstitial atom defect configurations[?] .

All the *ab initio* calculation were performed using Vienna Ab initio Simulation Package (VASP)[27–30] and the AM05[31–33] exchange-correlation functional. The plane wave energy cutoff was 450 eV. In order to investigate the cell size effect, we explored different sizes of simulation cells. For simulation cells containing 4x4x4 bcc unit cells, we used 5x5x5 k-points. In the simulations involving 4x4x5 bcc unit cells, we used a 5x5x4 k-point mesh.

First, perfect lattice simulation cells containing 128 atoms and 160 atoms for each element were fully relaxed. Then, we created cells containing 129 atoms and 161 atoms, with a self-interstitial atom defect in a $\langle 111\rangle$ crowdion configuration. Atomic positions were then relaxed, but the cell size and shape was kept the same as in the perfect lattice case. Elastic dipole tensors for all the metals were computed from macro-stresses, using equation (27). The results are given in Table I.

We have also computed defect dipole tensors using equation (21). Simulation cells containing $\langle 111\rangle$ self-interstitial defects were fully relaxed, such that the macro-stress vanished, $\langle\sigma_{ij}\rangle = 0$. The sizes of simulation cells are now different from the perfect lattice cases, and the deformation of the cell has the same effect as an application of external strain. Numerical results are summarized in Table II. Elastic constants C_{ijkl} were calculated following the method proposed by Le Page and

129 atoms	P_{11}	P_{22}	P_{33}	P_{12}	P_{23}	P_{31}
W	53.84	53.84	53.84	13.23	13.23	13.23
Mo	40.37	40.37	40.37	7.814	7.814	7.814
Ta	34.68	34.68	34.68	6.645	6.645	6.645
Nb	31.69	31.69	31.69	3.001	3.001	3.001
V	21.28	21.28	21.28	-0.162	-0.162	-0.162
161 atoms	P_{11}	P_{22}	P_{33}	P_{12}	P_{23}	P_{31}
W	52.97	52.97	54.78	12.73	13.07	13.07
Mo	39.60	39.60	41.29	7.213	7.758	7.758
Ta	34.61	34.61	34.22	6.081	6.152	6.152
Nb	32.00	32.00	31.77	2.099	2.023	2.023
V	16.93	16.93	17.47	0.154	-0.132	-0.132

TABLE I: Elastic dipole tensors of $\langle 111 \rangle$ crowdion configurations for W, Mo, Nb, Ta and V. The values were computed using *ab initio* simulations with no relaxation of simulation cells. Values are given in eV units.

129 atoms	P_{11}	P_{22}	P_{33}	P_{12}	P_{23}	P_{31}
W	53.75	53.75	53.75	13.39	13.39	13.39
Mo	40.35	40.35	40.35	7.709	7.709	7.709
Ta	34.37	34.37	34.37	6.069	6.069	6.069
Nb	31.15	31.15	31.15	2.027	2.027	2.027
V	18.13	18.13	18.13	-0.179	-0.179	-0.179

TABLE II: Elastic dipole tensors of $\langle 111 \rangle$ crowdion configurations for W, Mo, Nb, Ta and V. The values were computed using *ab initio* simulations with full relaxation of simulation cells. Values are given in eV units.

Saxe[34], using a 2-atoms cell with 30x30x30 k-points. The values are given in Table III in Voigt notations.

The convergence of *ab initio* results is verified using molecular statics calculations using tungsten as an example. Calculations were performed using LAMMPS[35] and the interatomic tungsten potential (EAM4) developed by Marinica *et al.*[36]. We have followed a procedure similar to that outlined above. First, we have relaxed a number of perfect lattice simulation cells containing various numbers of atoms. Then, we produced a self-interstitial atom defect in a $\langle 111 \rangle$ configuration, and the relaxed atomic positions without relaxing the simulation cell itself. The results are summarized in Table IV. Values of elastic constants characterizing the interatomic potential were found to be the same as those given in Ref. 36, which are $C_{11} = 523$GPa, $C_{12} = 202$GPa and $C_{44} = 161$GPa. Results given in the table show that achieving full convergence requires using fairly large simulation cells, exceeding approximately by a factor of two the dimensions readily accessible to density functional theory calculations. Still, even with relatively small simulation cells, it is possible to compute the elements of dipole tensors at approximately $\sim$5% level of accuracy, sufficient for applications. This assessment of accuracy is confirmed by the analysis of solutions of the Frenkel-Kontorova model for the $\langle 111 \rangle$ defects given in[39] and illustrated in Fig. 3.

	a_0	C_{11}	C_{12}	C_{44}
W	3.149	569.73	211.52	157.16
Mo	3.124	505.43	175.26	108.04
Ta	3.278	293.44	168.18	82.08
Nb	3.282	273.54	143.06	23.62
V	2.956	308.53	147.96	31.31

TABLE III: Lattice parameters (in Angstrom units) and elastic constants (in GPa units) of W, Mo, Nb, Ta and V, calculated following Le Page and Saxe[34], using a 2-atom cell and 30x30x30 k-points.

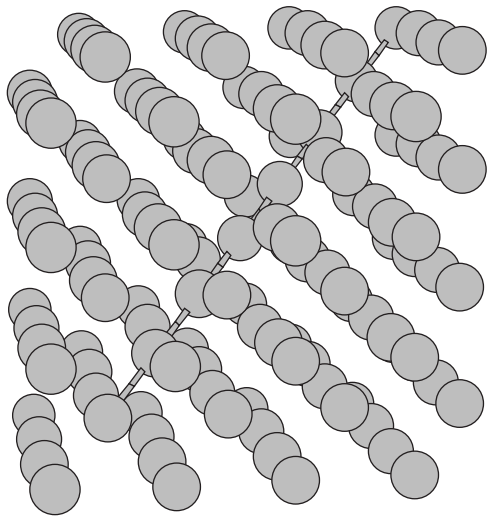

FIG. 2: Atomic structure of a self-interstitial atom defect in vanadium, where the orientation of the axis of the defect is close to the [111] direction. Atomic bonds are shown for the atoms that are significantly closer to each other than atoms in a perfect lattice, similarly to the case of tungsten illustrated in Fig. 1. Note that the strain field of a defect in vanadium is less localised than the strain field of tungsten.

V. ELASTIC FIELDS AND INTERACTIONS INVOLVING SIA DEFECTS

The energy of elastic interaction between two defects with elastic dipole tensors P^a_{ij} and P^b_{kl} in the isotropic elasticity approximation is given by equation (2), where the derivative of elastic Green's function (3) is

$$\begin{aligned} \frac{\partial}{\partial x_j}\frac{\partial}{\partial x_l}G_{ik}(\mathbf{r}) &= \frac{1}{16\pi\mu(1-\nu)r^3}\times \\ \times\ & [(3-4\nu)\delta_{ik}\,(3\eta_l\eta_j-\delta_{lj}) + 15\eta_i\eta_j\eta_k\eta_l \\ -\ & 3(\delta_{ij}\eta_k\eta_l+\delta_{il}\eta_j\eta_k+\delta_{jl}\eta_i\eta_k+\delta_{kj}\eta_i\eta_l+\delta_{kl}\eta_i\eta_j) \\ +\ & (\delta_{il}\delta_{kj}+\delta_{ij}\delta_{kl})]. \end{aligned} \tag{31}$$

In the above equation, η_i is a component of the radial unit vector $\boldsymbol{\eta} = \mathbf{r}/r$. Using expression (19) for the elastic

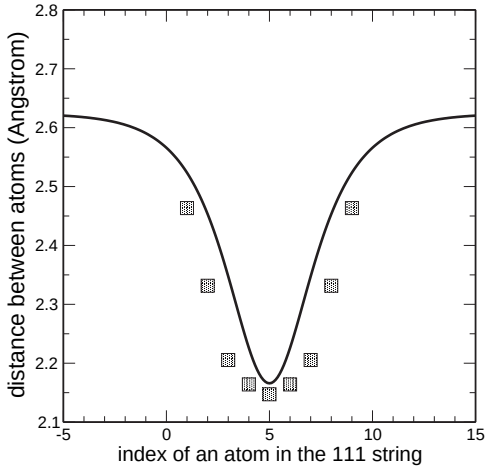

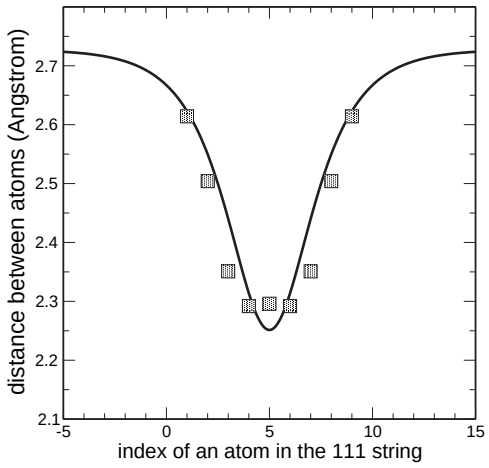

FIG. 3: Distances between atoms in the ⟨111⟩ most strongly distorted atomic strings in vanadium (top) and tungsten (bottom). Continuous lines are the solutions of the Frenkel-Kontorova model[39], points are the distances derived from DFT simulations. In agreement with the data given in table IV, the Frenkel-Kontorova solutions show that to achieve convergence, atomistic calculations require a simulation cell of the size approximately twice that of cells normally used in DFT calculations.

dipole tensors of interacting defects, from (2) we find

$$\begin{aligned} E_{int} &= \frac{\mu\left(\Omega^{(1)}\right)^2}{4\pi(1-\nu)r^3}\left[-12\nu(\boldsymbol{\eta}\cdot\mathbf{e})(\boldsymbol{\eta}\cdot\mathbf{n})(\mathbf{e}\cdot\mathbf{n})\right. \\ &+ 2(2\nu-1)(\mathbf{e}\cdot\mathbf{n})^2 + 15(\boldsymbol{\eta}\cdot\mathbf{e})^2(\boldsymbol{\eta}\cdot\mathbf{n})^2 \\ &+ \left. 1 - 3(\boldsymbol{\eta}\cdot\mathbf{e})^2 - 3(\boldsymbol{\eta}\cdot\mathbf{n})^2\right] \\ &+ \frac{\mu}{2\pi(1-\nu)r^3}\Omega^{(1)}\left[\nu\Omega^{(1)} + \frac{(1+\nu)}{3}\Omega^{(2)}\right] \\ &\times \left\{\left[3(\boldsymbol{\eta}\cdot\mathbf{e})^2-1\right] + \left[3(\boldsymbol{\eta}\cdot\mathbf{n})^2-1\right]\right\}, \end{aligned} \tag{32}$$

where vectors $\mathbf{n}$ and $\mathbf{e}$ define orientations of the two interacting anisotropic defects. If the orientation unit vectors

Box size	P_{11}	P_{22}	P_{33}	P_{12}	P_{23}	P_{31}
4x4x4	36.99	36.99	36.99	17.35	17.35	17.35
4x4x5	37.76	37.76	37.18	17.33	16.96	16.96
5x5x5	38.71	38.71	38.71	18.26	18.26	18.26
5x5x6	37.80	37.80	37.85	17.10	16.91	16.91
7x7x7	37.54	37.54	37.54	16.68	16.68	16.68
7x7x8	37.48	37.48	37.51	16.66	16.61	16.61
10x10x10	37.32	37.32	37.32	16.58	16.58	16.58
10x10x11	37.30	37.30	37.31	16.58	16.57	16.57
20x20x20	37.19	37.19	37.19	16.58	16.58	16.58
20x20x22	37.19	37.19	37.19	16.59	16.58	16.58
50x50x50	37.17	37.17	37.17	16.59	16.59	16.59
50x50x55	37.17	37.17	37.17	16.59	16.59	16.59
100x100x110	37.16	37.16	37.16	16.59	16.59	16.59

TABLE IV: Dipole tensors of ⟨111⟩ self-interstitial defect configurations in W computed using Marinica EAM4 potential[36]. The values were found using molecular statics and no relaxation of simulation cells. Values are given in eV units.

	Ω_0	$\Omega^{(1)}$	$\Omega^{(2)}$	Ω_{rel}	Ω_{rel}/Ω_0
W	15.61	20.23	5.84	26.07	1.67
	15.61	20.48	5.55	26.02	1.67
Mo	15.61	17.38	5.29	22.67	1.45
	15.61	17.15	5.51	22.66	1.45
Ta	17.62	19.46	7.01	26.47	1.50
	17.62	17.77	8.46	26.23	1.49
Nb	17.68	30.46	-3.24	27.22	1.54
	17.68	20.57	6.18	26.75	1.51
V	12.91	-1.24	18.17	16.92	1.31
	12.91	-1.37	15.79	14.42	1.12

TABLE V: Equilibrium atomic volume $\Omega_0 = a_0^3/2$, parameters $\Omega^{(1)}$ and $\Omega^{(2)}$ of elastic dipole tensor of a defect (17), the total elastic relaxation volume of the defect, and the same quantity expressed as a fraction of equilibrium atomic volume. All the dimensional values are given in cubic Angstrom units. The first row for each metal shows values computed using the zero strain method, the second row gives values computed using the zero stress method. The elastic relaxation volume of a self-interstitial defect in tungsten given in the table agrees almost exactly with the value found earlier in Ref. 37.

of the two defects are parallel $\mathbf{n}\|\mathbf{e}$, formula (32) acquires a particularly simple form

$$\begin{aligned} E_{int} &= \frac{\mu\left(\Omega^{(1)}\right)^2}{4\pi(1-\nu)r^3}\left[15(\boldsymbol{\eta}\cdot\mathbf{n})^4 - 6(\boldsymbol{\eta}\cdot\mathbf{n})^2 - 1\right] \\ &+ \frac{\mu\Omega^{(1)}\Omega^{(2)}}{3\pi r^3}\frac{(1+\nu)}{(1-\nu)}\left[3(\boldsymbol{\eta}\cdot\mathbf{n})^2-1\right]. \end{aligned} \tag{33}$$

There is a striking similarity between this equation and equations describing elastic interaction between two prismatic dislocation loops, and between a prismatic dislocations loop and a dilatation centre, for example a vacancy. The first term in (33) is identical to equation (18) of Ref. 38, and the second term is similar to equation (16) of Ref. 14. The energy of elastic interaction between anisotropic

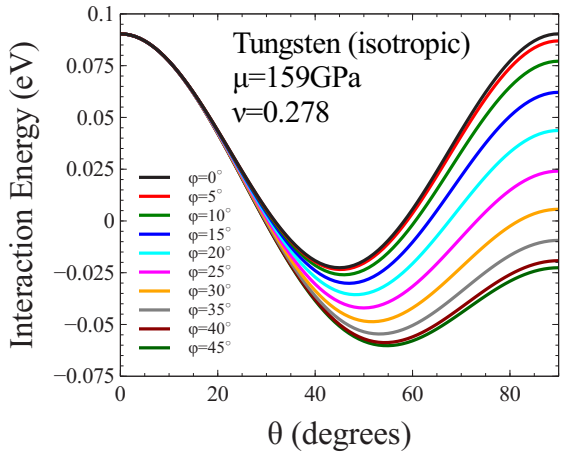

FIG. 4: (Color online) Energy of elastic interaction between a ⟨111⟩ self-interstitial atom defect and its images in tungsten as a function of the orientation of vector **n**, computed using data from Table V in the isotropic elasticity approximation.

defects (32) is strongly angularly dependent, and is maximum for the orientations where vector **n** is parallel to $\boldsymbol{\eta}$.

VI. ELASTIC ENERGY OF A PERIODIC ARRAY OF DEFECTS

The energy of elastic interaction of a defect with its images in periodic boundary condition simulation can be evaluated as

$$E_{int}^{total} = \frac{1}{2}\sum_n E_{int}^{(n)}(\mathbf{r}_n), \qquad (34)$$

where $\mathbf{r}_n$ is the radius-vector from a defect to its image n. $E_{int}^{(n)}$ in the isotropic elasticity limit is given by equation (33). In the anisotropic elasticity approximation, the energy can be computed using equation (2), where elastic Green's function and its second derivative $G_{ik,jl}$ can be evaluated using the method developed by Barnett[40].

Using the values of parameters $\Omega^{(1)}$ and $\Omega^{(2)}$ given in Table V, we evaluate dipole tensor P_{ij} of a ⟨111⟩ defect as a function of orientation of its directional unit vector **n**. Fig. 4 shows the energy of elastic interaction of a ⟨111⟩ defect with its periodic images in tungsten, computed using isotropic elasticity for a $4 \times 4 \times 4$ periodically translated set of unit cells. The data shown in the Figure were computed assuming μ=159GPa and ν=0.278. Summation over neighbouring cells involved twenty nearest neighbour defects. The minimum of elastic energy corresponds to spherical angles $\phi = 45°$ and $\theta = 54.7356° = \cos^{-1}(1/\sqrt{3})$, which correspond to the [111] crystallographic direction.

We have also computed the energy of elastic interaction E_{int}^{total} in the anisotropic elasticity approximation, using

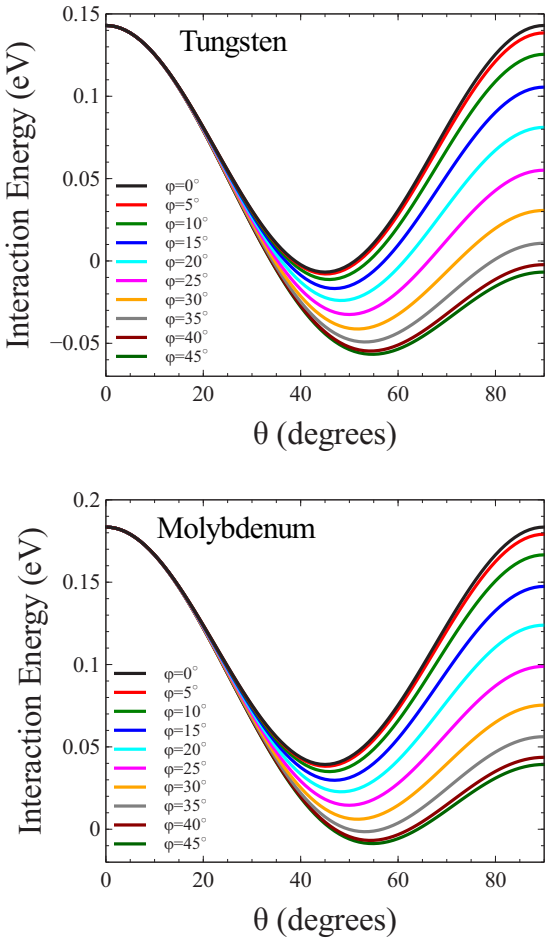

FIG. 5: (Color online) The energy of elastic interaction between a ⟨111⟩ self-interstitial atom defect and its periodic images as a function of the orientation of vector **n**, computed in the full anisotropic elasticity approximation for tungsten (top) and molybdenum (bottom).

equation (2) and evaluating the elastic Green's function numerically, following Ref. 40. We find that for all the bcc transition metals, the most elastically favourable orientation of a self-interstitial defect, computed assuming periodically translated cubic simulation cells, corresponds to the ⟨111⟩ orientation of the axis of the defect.

VII. SUMMARY AND CONCLUSIONS

We have derived analytical formulae for the elastic dipole tensors of ⟨111⟩ self-interstitial atom defects, using isotropic and anisotropic elasticity approximations. The equations show that, in addition to the prismatic dislocation loop-like character, the elastic field of a ⟨111⟩ defect has a significant isotropic dilatation component. Using DFT calculations, we parameterize dipole tensors of defects for all the non-magnetic bcc transition metals. We then use the data to evaluate the energy of elastic inter-

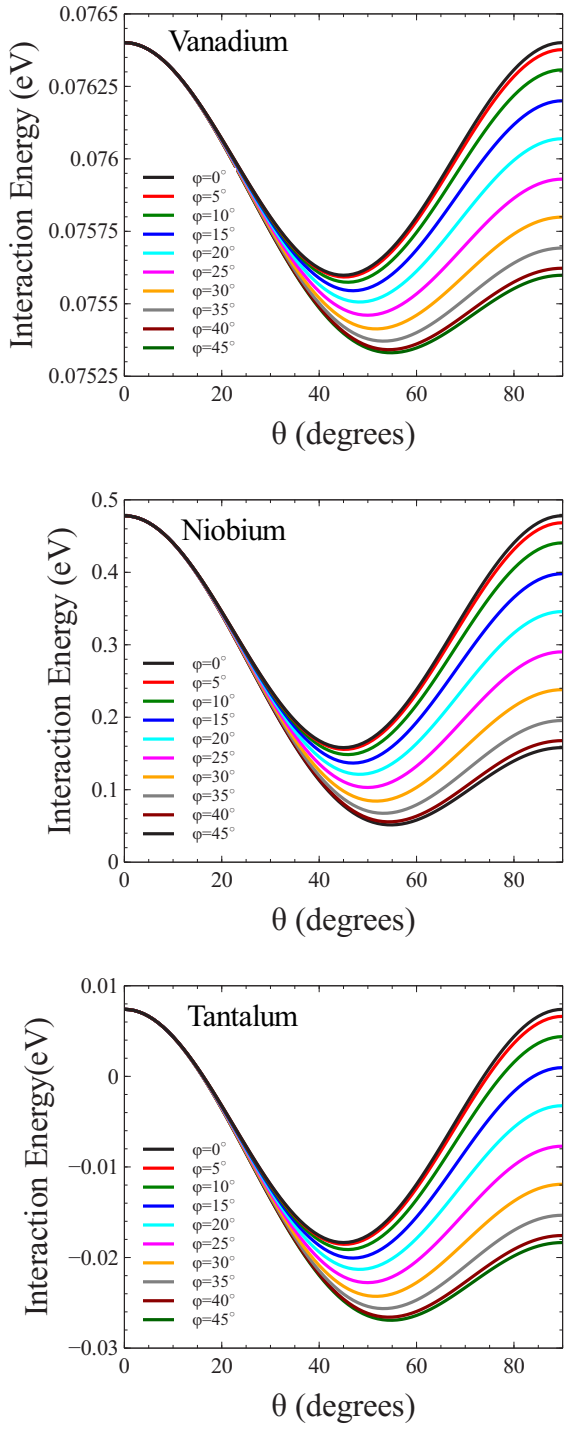

FIG. 6: (Color online) The energy of elastic interaction between a ⟨111⟩ self-interstitial atom defect and its periodic images as a function of the orientation of vector **n**, computed in the full anisotropic elasticity approximation for vanadium (top), niobium (middle) and tantalum (bottom).

action between the defects that shows that in a periodic three-dimensional arrangement, long-range elastic interactions between the defects favour the ⟨111⟩ orientation of their axis, an effect resulting from the interaction between a defect and all its images in a simulation involving periodic boundary conditions.

Acknowledgments

This work was part-funded by the RCUK Energy Programme (Grant Number EP/P012450/1) and by the European Unions Horizon 2020 research and innovation programme under grant agreement number 633053. To obtain further information on the data and models underlying this paper please contact PublicationsManager@ukaea.uk. The views and opinions expressed herein do not necessarily reflect those of the European Commission. We are grateful to C.-H. Woo and A.P. Sutton for the discussions that stimulated this study.

* Electronic address: sergei.dudarev@ukaea.uk

[1] S. Han, L. A. Zepeda-Ruiz, G. J. Ackland, R. Car, and D.

J. Srolovitz, *Self-interstitials in V and Mo*, Phys. Rev. B **66**, 220101 (2002).
[2] D. Nguyen-Manh, A. P. Horsfield, and S. L. Dudarev, *Self-interstitial atom defects in bcc transition metals: Group-specific trends*, Phys. Rev. B **73**, 020101 (2006).
[3] P. M. Derlet, D. Nguyen-Manh, S. L. Dudarev, *Multiscale modeling of crowdion and vacancy defects in body-centered-cubic transition metals*, Phys. Rev. B **76**, 054107 (2007).
[4] S.L. Dudarev, *Density Functional Theory Models for Radiation Damage*, Annu. Rev. Mater. Res. **43**, 35 (2013).
[5] A. R. Allnatt, *Crystal Lattice Defects and Matter Transport*, in: E. Abecassis de Loredo and N. K. Jurisic (Eds.), Selected Topics in Physics, Astrophysics, and Biophysics, Proceedings of the XIV Latin American School of Physics, Caracas 10-28 July 1972, vol. **3-43**, pp. 3–42 (Kluwer Academic Publishers, 1973).
[6] A.E. Sand, K. Nordlund, and S.L. Dudarev, *Radiation damage production in massive cascades initiated by fusion neutrons in tungsten*, J. Nucl. Mater. **455** (2014) 207
[7] A.E. Sand, M.J. Aliaga, M.J. Caturla and K. Nordlund, *Surface effects and statistical laws of defects in primary radiation damage: Tungsten versus iron*, EPL **115** (2016) 36001
[8] M. W. Thompson, *The Damage and Recovery of Neutron Irradiated Tungsten*, Philos. Mag. **5**, 278 (1960).
[9] F. Dausinger and H. Schultz, *Long-Range Migration of Self-Interstitial Atoms in Tungsten*, Phys. Rev. Lett. **35**, 1773 (1975)
[10] T.D. Swinburne, P.-W. Ma, and S.L. Dudarev, *Low temperature diffusivity of self-interstitial defects in tungsten*, New J. Phys. **19**, 073024 (2017).
[11] S.L. Dudarev, *The non-Arrhenius migration of interstitial defects in bcc transition metals*, Comptes Rendus Physique **9**, 409 (2008)
[12] T. D. Swinburne, S. L. Dudarev, and A. P. Sutton, *Classical Mobility of Highly Mobile Crystal Defects*, Phys. Rev. Lett. **113**, 215501 (2014)
[13] T. D. Swinburne and S. L. Dudarev, *Phonon drag force acting on a mobile crystal defect: Full treatment of discreteness and nonlinearity*, Phys. Rev. B**92**, 134302 (2015)
[14] S.L. Dudarev and A.P. Sutton, *Elastic interactions between nano-scale defects in irradiated materials*, Acta Materialia **125**, 425 (2017)
[15] J. P. Hirth and J. Lothe, *Theory of Dislocations*, (Krieger, Malabar, 1992).
[16] J. Marian, B.D. Wirth, J. M. Perlado, G.R. Odette, and T. Diaz de la Rubia, *Dynamics of self-interstitial migration in Fe-Cu alloys*, Phys. Rev. B **64**, 094303 (2001)
[17] Z. Chen, N. Kioussis, N. Ghoniem, and D. Seif, *Strain-field effects on the formation and migration energies of self interstitials in α-Fe from first principles*, Phys. Rev. B**81**, 094102 (2010)
[18] G. Leibfried and N. Breuer, *Point Defects in Metals*, (Springer, Berlin, 1978), pp. 145-164
[19] L. Ventelon, F. Willaime, C.-C. Fu, M. Heran, and I. Ginoux, *Ab initio investigation of radiation defects in tungsten: Structure of self-interstitials and specificity of di-vacancies compared to other bcc transition metals*, J. Nucl. Mater. bf 425, 16 (2012)
[20] T. Mura, *Micromechanics of defects in solids* (Kluwer, Dordrecht, 1991) p.22
[21] L.D. Landau and E.M. Lifshits, *Theory of Elasticity*, 3rd Edition. (Butterworth-Heinemann, Oxford, 1986) p.112
[22] J. F. Nye, *Physical Properties of Crystals*, (Oxford University Press, Oxford, England, 1985).
[23] T. D. Swinburne, K. Arakawa, H. Mori, H. Yasuda, M. Isshiki, K. Mimura, M. Uchikoshi and S. L. Dudarev, *Fast, vacancy-free climb of prismatic dislocation loops in bcc metals*, Scientific Reports **6**, 30596 (2016)
[24] I. Rovelli, S.L. Dudarev, A.P. Sutton, *Non-local model for diffusion-mediated dislocation climb and cavity growth*, Journal of the Mechanics and Physics of Solids **103**, 121 (2017)
[25] E. Clouet, S. Garruchet, H. Nguyen, M. Perez, C. S. Becquart, *Dislocation interaction with C in α-Fe: A comparison between atomic simulations and elasticity theory*, Acta Mater. **56**, 3450 (2008)
[26] C. Varvenne, F. Bruneval, M.-C. Marinica and E. Clouet, *Point defect modeling in materials: Coupling ab initio and elasticity approaches*, Phys. Rev. B **88**, 134102 (2013)
[27] G. Kresse and J. Hafner, Phys. Rev. B, **47** 558, (1993).
[28] G. Kresse and J. Hafner, Phys. Rev. B, **49** 14251, (1994).
[29] G. Kresse and J. Furthmüller, Comput. Mat. Sci., **6** 15, (1996).
[30] G. Kresse and J. Furthmüller, Phys. Rev. B, **54** 11169, (1996).
[31] R. Armiento and A. E. Mattsson, Phys. Rev. B **72**, 085108 (2005).
[32] A. E. Mattsson and R. Armiento, Phys. Rev. B **79**, 155101 (2009).
[33] A. E. Mattsson, R. Armiento R, J. Paier, G. Kresse, J. M. Wills, and T. R. Mattsson, J. Chem. Phys **128**, 084714 (2008).
[34] Y. Le Page and P. Saxe, Phys. Rev. B **65**, 104104 (2002)
[35] S. Plimpton, J Comp Phys, **117**, 1 (1995); http://lammps.sandia.gov/
[36] M.-C. Marinica, L. Ventelon, M. R. Gilbert, L. Proville, S. L. Dudarev, J. Marian, G. Bencteux and F. Willaime, *Interatomic potentials for modelling radiation defects and dislocations in tungsten*, J. Phys.: Conden. Matt. **25**, 395502 (2013)
[37] F. Hofmann, D. Nguyen-Manh, M.R. Gilbert, C.E. Beck, J.K. Eliason, A.A. Maznev, W. Liu, D.E.J. Armstrong, K.A. Nelson and S.L. Dudarev, *Lattice swelling and modulus change in a helium-implanted tungsten alloy: X-ray micro-diffraction, surface acoustic wave measurements, and multiscale modelling*, Acta Materialia **89**, 352 (2015)
[38] S. L. Dudarev, M. R. Gilbert, K. Arakawa, H. Mori, Z. Yao, M. L. Jenkins and P. M. Derlet, *Langevin model for real-time Brownian dynamics of interacting nanodefects in irradiated metals*, Phys. Rev. B **81**, 224107 (2010)
[39] S.L. Dudarev, *Coherent motion of interstitial defects in a crystalline material*, Philosophical Magazine **83**, 3577 (2003)
[40] D. M. Barnett, Phys. Stat. Sol. (b) **49**, 741 (1972)